International Journal of Precision Engineering and Manufacturing-Green Technology
https://doi.org/10.1007/s40684-026-00909-2

Online ISSN 2198-0810
Print ISSN 2288-6206issn_last

REGULAR PAPER

ALOHA-DED: A Low-cost Open-source Hardware Architecture for Directed Energy Deposition Enabling In-Situ Thermal Control and Enhanced Microstructural and Mechanical Performance

Mohammad Rezazadeh[1] · Ji-Won Lim[1] · Hong-Seok Kim[2] · Geon-Ju Kim[3] · Melkamu Tadesse Getachew[1] · Do-Sik Sim[4] · Sang-Hu Park[3]

Received: 19 December 2025 / Revised: 1 May 2026 / Accepted: 2 June 2026

Abstract

Directed Energy Deposition (DED) is a powerful metal additive manufacturing process, yet it frequently suffers from heat accumulation and unstable thermal cycles that lead to geometric distortion, excessive penetration, and heterogeneous microstructures. To address these limitations and avoid the restricted control of commercial systems, this study presents A Low-cost, Open-source Hardware Architecture for DED, referred to as ALOHA-DED. The platform provides full access to hardware signals and real-time actuation, enabling advanced sensing and adaptive control capabilities that are not feasible on proprietary machines. A non-contact off-axis pyrometer was integrated for continuous melt pool temperature monitoring, and a Proportional–Integral–Derivative controller implemented on Digital Signal Processor-based controller that leverages a Field-Programmable Gate Array for high-speed hardware acceleration. Experiments using stainless steel 316 L powder demonstrated that the closed-loop thermal control effectively suppresses thermal runaway. During thin-wall fabrication, open-loop deposition exhibited a thermal drift greater than 300 °C, whereas the closed-loop system maintained a stable melt pool temperature of 1800 °C by automatically reducing laser power by approximately 40%. This resulted in a controlled conduction-mode melt pool, refined grain structure, and a 20–30% increase in micro-hardness. These findings confirm that pyrometry-based closed-loop thermal control substantially improves thermal stability and build quality in DED processes.

Keywords Directed energy deposition · Closed loop control · In-situ monitoring · Melt pool temperature · Mechanical properties

✉ Sang-Hu Park
sanghu@pusan.ac.kr

1 Graduate School of Mechanical Engineering, Pusan National University, Geumjeong-gu, Busan 46241, Korea

2 Research Institute of Mechanical Technology, Pusan National University, Busan, Republic of Korea

3 School of Mechanical Engineering, Pusan National University, Geumjeong-gu, Busan 46241, Korea

4 Department of Ocean Advanced Materials Convergence Engineering, Korea Maritime & Ocean University, Busan, Republic of Korea

1 Introduction

Directed Energy Deposition (DED) is widely used for manufacturing and repairing high-value metallic components [1]; however, its process stability remains strongly limited by rapid thermal transients, repeated reheating, and geometry-dependent heat flow [2, 3]. These effects lead to substantial fluctuations in melt-pool temperature, which in turn influence penetration mode, dilution, microstructure evolution, and dimensional fidelity [4, 5]. Numerous works have identified thermal instability and heat accumulation as primary barriers to achieving consistent, repeatable quality in DED builds [4, 6]. Because melt-pool temperature directly governs solidification dynamics, researchers have emphasized the need for real-time temperature regulation to ensure stable processing conditions [7, 8].

Several approaches have been explored to monitor, regulate, and utilize melt pool behavior in Directed Energy Deposition. Early and ongoing studies have primarily focused on direct melt pool temperature control using feedback strategies such as predictive control with dual color pyrometry [9, 10] and rule based, model based, or feed-forward feedback controllers to improve robustness under dynamic thermal conditions [11, 12]. A wide range of sensing modalities, including pyrometers, infrared cameras [13], and hyperspectral systems, have been employed to capture melt pool temperature fields, thermal gradients, and transient disturbances during deposition [8, 14]. More recently, data driven and machine learning approaches have been introduced to model complex nonlinear relationships between process parameters and deposition outcomes such as bead geometry and shape, even under limited experimental data conditions [15]. These works collectively demonstrate the importance of high-bandwidth thermal feedback and adaptive power modulation for achieving stable process behavior. While these studies have established the importance of thermal monitoring and control, prior work varies widely in scope, capability, and limitations. A more detailed examination of these research efforts further highlights the gaps addressed in the present study.

Early research efforts demonstrated the feasibility of regulating melt-pool temperature in laser-based deposition yet offered limited insight into resulting material properties. Song and Mazumder [9] developed one of the first closed-loop temperature controllers using a dual-color pyrometer and model-predictive control to stabilize melt-pool temperature during laser cladding; however, the evaluation focused solely on thermal tracking and geometric compensation, without examining microstructural evolution or hardness changes. Similarly, classical height-regulation studies such as Tang and Landers [16] employed optical sensing and iterative learning algorithms to maintain layer height but did not attempt to control melt-pool temperature or relate process stabilization to material quality. These early works highlight foundational progress in thermal or geometric control, yet leave unresolved how real-time temperature regulation influences microstructure, mechanical consistency, and defect formation in DED.

More recent studies have advanced melt-pool temperature control architectures but continued to emphasize control performance rather than material properties. Liao et al. [12] proposed a simulation-guided feedforward–feedback framework that improved temperature tracking accuracy, yet the work did not investigate how thermal regulation affects grain morphology, porosity, or hardness. Likewise, high-speed sensing and (Field-Programmable Gate Array (FPGA)-based implementations introduced by Sanchez-Medina et al. [17] demonstrated real-time temperature estimation using hyperspectral imaging and evaluated controller-gain effects on melt-pool dimensions, but offered no microstructural or mechanical characterization. Studies on thermal-history estimation such as Nair et al. [8] and hyperspectral thermal analysis by Sanchez-Medina et al. [18] focused on sensing improvements rather than closed-loop material-property control. Thus, despite technical sophistication, these works did not establish how temperature stability translates into microstructural uniformity or mechanical improvements.

Among previous studies, Smoqi et al. [11] most closely examined the connection between thermal control and material response by demonstrating that closed-loop power modulation can reduce porosity variation and promote more consistent dendritic microstructure in 316 L stainless steel. However, their system operated at a low sampling frequency and was implemented on a closed, commercial machine, limiting control bandwidth, responsiveness, and the ability to explore thermal transients in complex geometries. Furthermore, the study did not systematically evaluate spatial hardness variation or correlate temperature stability with solidification behavior. These limitations underscore a broader gap in understanding how high-bandwidth, open-architecture temperature control influences melt-pool stability, microstructural uniformity, and mechanical properties across both simple and complex deposition paths.

Despite this progress, significant limitations remain uninvestigated as needed. Most prior research relies on commercial DED machines, which typically operate as closed, proprietary systems. These platforms restrict user access to internal control logic, sensing channels, real-time actuation pathways, and laser-power command interfaces, making it difficult to implement or test custom high-speed control strategies. Reviews consistently highlight that such “black-box” architectures hinder scientific exploration of advanced controllers, multi-sensor fusion, and physics-informed regulation [4, 5]. Furthermore, the cost of industrial monitoring and control hardware coaxial sensors, high-speed controllers, and multi-modal sensing packages poses an additional barrier for many research laboratories. There remains a clear need for affordable, open, and fully accessible platforms that allow real-time experimentation with melt-pool control algorithms.

To address this gap, the present work develops ALOHA-DED, a low-cost and fully open-architecture laser DED platform that provides unrestricted access to all hardware and sensing interfaces. Building on this transparent architecture, a pyrometry-based closed-loop temperature control system is implemented using a high-bandwidth FPGA/Digital Signal Processor (DSP) controller capable of sub-millisecond laser-power modulation. Using this system, the study evaluates how closed-loop thermal stabilization influences

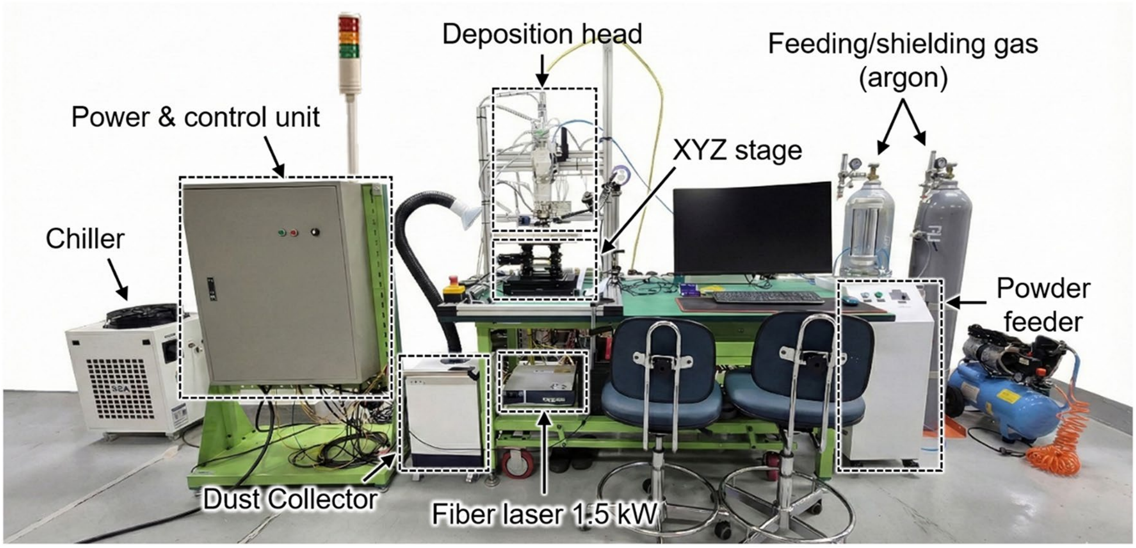

Fig. 1 ALOHA DED, a customized DED system as a lab version. Every component is designed and installed in-house

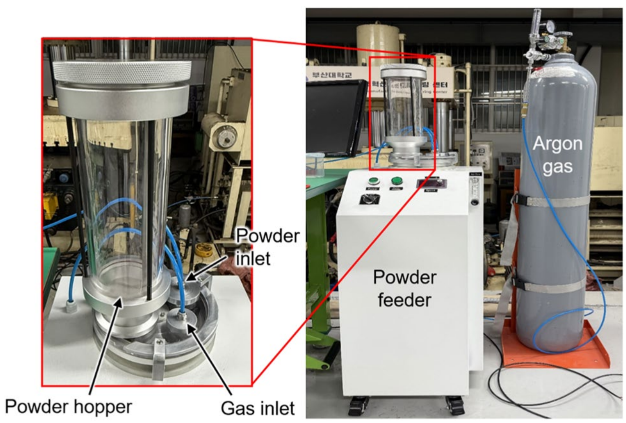

Fig. 2 Powder feeder, single hopper and argon gas in the ALOHA DED system

deposition behavior across single-line and thin-wall builds, and further examines how improved temperature stability affects homogeneity in microstructure and microhardness compared with open-loop processing.

2 ALOHA-DED System Development

2.1 System Overview and Hardware Architecture

The ALOHA-DED platform shown in Fig. 1 was designed as a fully open research-oriented DED system with complete access to sensing, actuation, and control signals. The system integrates four major subsystems: a fiber-laser heat source, a three-axis positioning stage, a coaxial powder-feeding system, and a high-speed controller. A 1.5 kW continuous-wave fiber laser (RFL-C020H-CE; Raycus, China) delivers energy through a 100 µm fiber through an optical head, producing a nominal 1.2 mm spot size at a 19 mm standoff distance.

Material delivery is provided through a single hopper powder feeder shown in Fig. 2, which delivers a stable and controllable mass flow of SS316L powder. The feeder exhibits linearity between dial setting and mass flow, verified experimentally through calibration, ensuring reproducibility across trials. Powder is transported using argon carrier gas and injected into the melt pool through a discrete three-jet coaxial delivery. Shielding gas is incorporated to prevent oxidation during deposition.

2.2 Control System Architecture

The core of the ALOHA-DED control system is a Dynomotion KFLOP board (KFLOP; Dynomotion, USA) shown in Fig. 3A, which integrates FPGA-level timing with DSP-based computation to provide deterministic, microsecond-resolution coordination of all process subsystems. The overall signal flow and connectivity between these system components are schematically illustrated in Fig. 3B. Unlike PC-based controllers that suffer from software jitter and non-deterministic scheduling, the KFLOP executes all motion, sensing, and actuation routines internally through low-level C code. This architecture enables custom interrupt routines, high-frequency control loops, and precise synchronization between the scanning motion, pyrometer acquisition, and laser-power modulation capabilities essential for investigating closed-loop thermal regulation in rapidly changing melt-pool conditions.

Complementing the KFLOP is the KANALOG interface module, which provides the analog and digital pathways

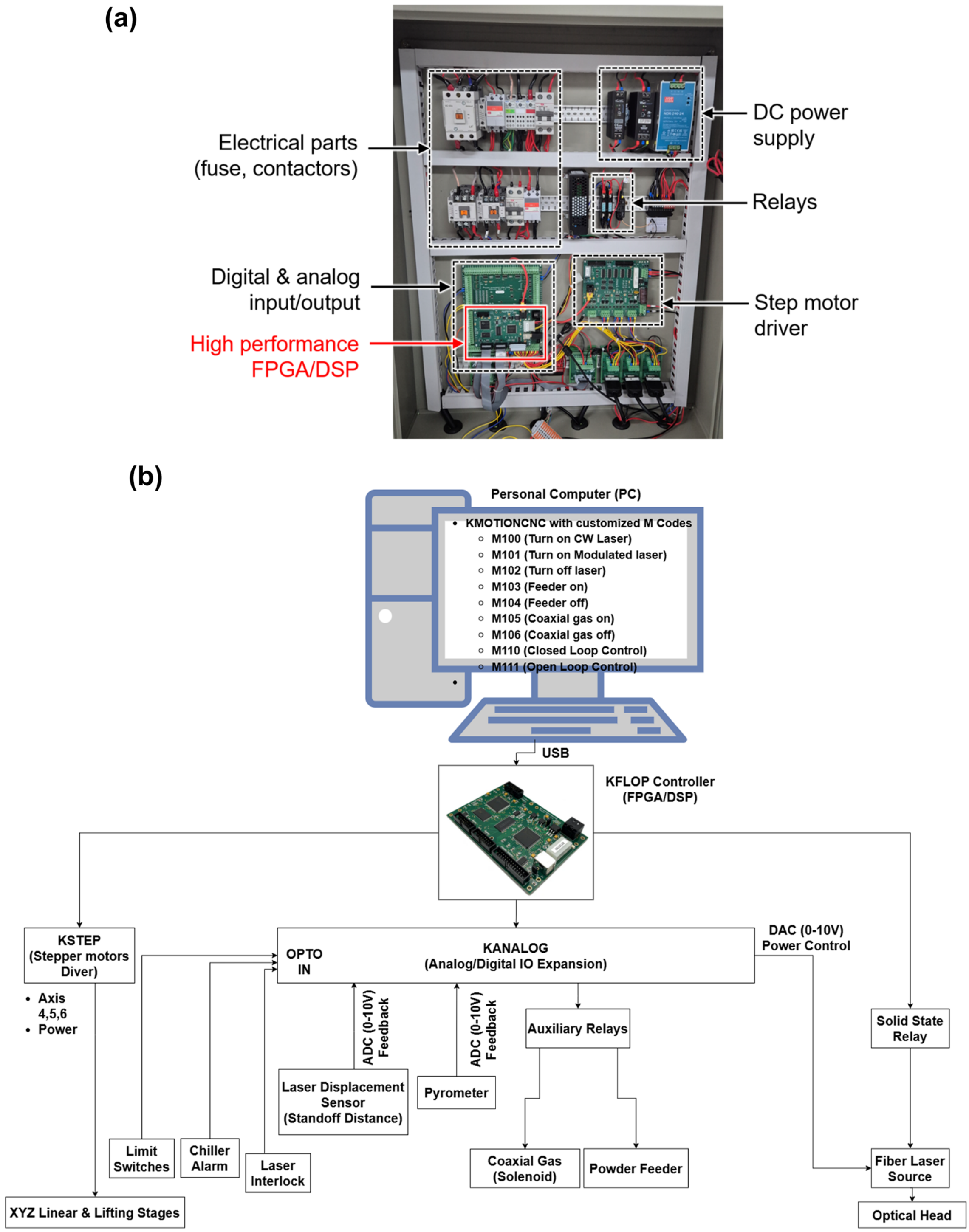

Fig. 3 **(A)** Physical Implementation of ALOHA DED power and control panel, **(B)** schematic of ALOHA DED system signal flow

required for driving the laser, powder feeder, shielding-gas valves, and external sensors. Its high-resolution Digital-to-Analog Converter (DAC) generate the 0–10 V analog command signal for continuous laser-power control, while dedicated relays enable energy modulation when needed. Digital Input/Output (I/O) lines control powder-feed triggering and gas flow, and the KSTEP (KSTEP; Dynomotion, USA) driver receives synchronized step-and-direction signals for precise XYZ motion. Because all actuation channels are hardware-timed through the KFLOP–KANALOG (KANALOG; Dynomotion, USA) pair, the system maintains precise alignment between process commands

Table 1 Chemical compositions SS316L powder

Fe (wt%)	Cr (wt%)	Ni (wt%)	Mo (wt%)	Mn (wt%)	Si (wt%)	*P* (wt%)	S (wt%)	C (wt%)
Bal.	16.00–18.00	12.00–15.00	2.00–3.00	2.00 max	1.00 max	0.045 max	0.030 max	0.030 max

Table 2 Particle size of SS316L powder

Particle size (50–150 µm)	D10 (µm)	D50 (µm)	D90 (µm)
	45–60	70–95	120–155

and physical responses, even under fast thermal or geometric transients. Also, the KFLOP and KANALOG form a fully accessible, high-bandwidth control backbone that distinguishes ALOHA-DED from closed commercial platforms. Every sensor input and actuator output is available to the user in real time, enabling direct implementation of advanced process-control strategies such as pyrometry-driven Proportional–Integral–Derivative (PID), multi-sensor fusion, or geometry-aware overrides. The determinism of the control hardware ensures that sensor readings, toolpath execution, and laser-power updates remain tightly synchronized at sub-millisecond scales, establishing a reliable foundation for adaptive melt-pool management and high-fidelity thermal stabilization during DED.

2.3 Real-Time Monitoring Subsystem

A single-color pyrometer (SWIFT 350 FO PL; AST, Israel) is integrated into the ALOHA-DED platform to provide continuous, high-frequency melt-pool temperature measurement essential for closed-loop thermal control. The sensor is mounted off-axis, and its optical path is configured to achieve a ~ 0.5 mm measurement spot fully within the melt-pool region. Although single-color pyrometry requires a fixed emissivity assumption (0.14 used in this work), its simplicity and responsiveness make it highly compatible with the open hardware architecture. The analog voltage output is sampled by a dedicated KFLOP thread, where it is converted into calibrated temperature data in real time, supplying the controller with the continuous thermal signature necessary for fast, stable PID-based power modulation.

Table 4 Open-Loop Single line laser scanning parameters

Test No.	Laser Power (W)	Scan Speed (mm/min)	Temperature (°C)	Standard Deviation (°C)	Steady-state error (°C)
1	647.1	900	1445.5	44.2	45.5
2	804.8	900	1590.6	51.6	9.4
3	995.5	900	1775.3	67.9	24.7
4	1204.8	900	1981.7	71.1	18.3

2.4 Toolpath Generation and Process Programming

A custom C# language based toolpath generator was developed to create fully programmable trajectories using parametric definitions of hatch spacing, layer height, scan direction, and inter-layer transitions. Instead of relying on external slicing software, the generator constructs toolpaths directly from user-defined geometric rules and embeds all laser, motion, and powder-feed commands into machine-ready instructions. This approach ensures consistent standoff control and stable energy input across varying build geometries, while also enabling precise experimental manipulation of deposition patterns.

During fabrication, the KFLOP controller interprets and executes the toolpath in real time, synchronizing motion with laser-power modulation and powder-flow activation. Because sensing and actuation are tightly integrated, the controller can modify laser power, adjust timing, or apply motion corrections based on instantaneous feedback from the pyrometer. Robust error-handling routines continuously verify command integrity, communication status, and subsystem readiness, ensuring reliable execution even when adaptive overrides occur at high frequency. Together, this framework enables toolpaths that are not only predefined but also dynamically responsive to thermal condition during deposition.

Table 3 Closed-Loop Single line laser scanning parameters

Test No.	Temperature Setpoint (°C)	Scan Speed (mm/min)	Average Laser Power (W)	Average Temperature (°C)	Standard Deviation (°C)	Steady-state error (°C)
1	1400	900	647.1	1400.01	45.3	0.01
2	1600	900	804.8	1599.6	61.7	0.4
3	1800	900	995.5	1800.4	88.3	0.4
4	2000	900	1204.8	1999.5	123.2	0.5

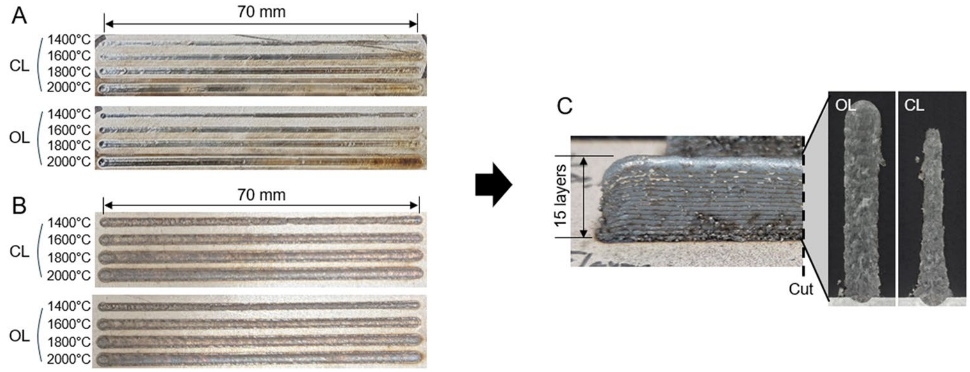

Fig. 4 **(A)** Single lines, without powder feeding to measure the surface temperature on a base plate according to laser power, **(B)** fabricated single lines, with powder feeding, and **(C)** comparison of thin-wall built up cases with and without laser power control. (CL: closed loop, OL: open loop)

Table 5 Closed-Loop Single line deposition parameters

Test No.	Temperature Setpoint (°C)	Scan Speed (mm/min)	Average Laser Power (W)	Average Temperature (°C)	Standard Deviation (°C)	Steady-state error (°C)
1	1400	900	455.9	1398.7	55.5	1.3
2	1600	900	777.5	1599.9	68.5	0.1
3	1800	900	1196.8	1800.0	100.1	0
4	2000	900	1499.9	1869.7	116.1	130.3

Table 6 Open-Loop Single line deposition parameters

Test No.	Laser Power (W)	Scan Speed (mm/min)	Temperature (°C)	Standard Deviation (°C)	Steady-state error (°C)
1	455.9	900	1391.6	77.4	8.4
2	777.5	900	1575.3	47.6	24.7
3	1196.8	900	1772.4	49.9	27.6
4	1499.9	900	1852.1	55.5	147.9

2.5 Closed-Loop Control Infrastructure

The closed-loop framework connects the pyrometer, controller, and laser through a < 1 ms feedback pipeline. Melt-pool temperature is sampled, compared to the setpoint, and translated into laser-power updates using an incremental PID controller running directly on the KFLOP. PID control was selected because its simple and transparent structure [30], ease of tuning, and proven robustness make it exceptionally well suited for real-time temperature regulation in DED [17, 31, 32], where system dynamics are difficult to model, the melt pool experiences continuous disturbances, and cost-effective yet highly reliable control is required [33–36]. Output clamping and corrective damping ensure stable convergence and prevent over-correction during transient disturbances. The controller's deterministic execution enables true real-time modulation of laser energy, providing the thermal stability required for reliable DED processing.

Safety mechanisms including thermal overshoot protection, watchdog routines for sensor dropouts, and emergency shutdown logic ensure robust operation under dynamic conditions. Together, the open hardware ecosystem, synchronized high-frequency sensing, and microsecond-responsive control framework establish ALOHA-DED as a flexible platform for advanced research in process control, multi-sensor data fusion, and adaptive melt-pool management.

3 Experimental Methodology

3.1 ALOHA-DED Machine Setup

All experiments in this study were carried out using the custom ALOHA-DED platform described in Sect. 2. The system provides real-time access to sensor signals and deterministic control of laser power, enabling a tightly regulated thermal environment throughout deposition. During all trials, the laser operated with a nominal 1.2 mm spot size and a fixed 19 mm stand-off distance, while continuous argon shielding was supplied to maintain a consistent melt-pool atmosphere. The experimental arrangement ensured stable energy delivery, reproducible melt-pool formation, and reliable evaluation of the thermal-control strategy.

Melt-pool temperature was measured using a single-color pyrometer mounted off-axis. The optical path was adjusted to generate a 0.5 mm measurement spot fully contained within the melt pool, enabling high-resolution capture of temperature fluctuations. The pyrometer output voltage was converted to temperature using a calibrated linear mapping with a fixed emissivity of 0.14. This configuration provided a continuous thermal signal that served as the input for real-time control.

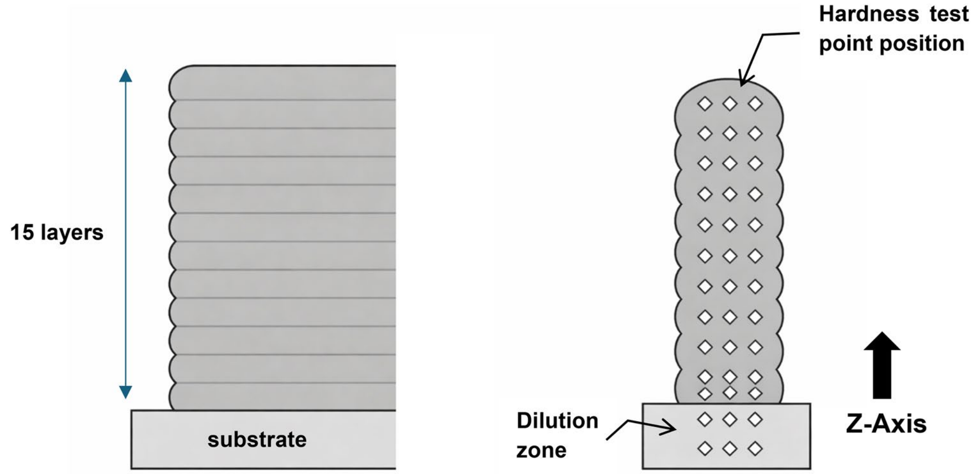

Fig. 5 Schematic of the hardness indentation points (15 built up layers (left), cross-sectional of the built up wall(right))

Closed-loop temperature stabilization was achieved through an incremental PID controller implemented directly on the KFLOP DSP. The controller continuously evaluated the deviation between the measured and target temperatures (1400–2000 °C) and updated the laser-power command through a 0–10 V analog output. The incremental form ensured smooth adjustments, minimized overshoot, and improved robustness against sensor noise. The proportional, integral, and differential gains were tuned experimentally using a heuristic approach to obtain rapid convergence and stable operation. This integrated experimental and control framework enabled consistent melt-pool behavior across all deposition conditions and provided a reliable basis for evaluating single-line and thin-wall fabrication under both open-loop and closed-loop operation.

3.2 Materials and Deposition Conditions

The feedstock material used in this study was SS316L powder with a particle-size range of 50 ~ 150 µm, supplied by HANA AMT Co. in Korea. Its chemical composition and size distribution are summarized in Table 1 and Table 2, respectively and all depositions were carried out on SS316L substrates measuring 50 × 150 × 10 mm. Across all experiments, the scanning speed, carrier-gas flow, and stand-off distance were kept constant to ensure consistent melt-pool formation. Laser power was applied either as a fixed value in open-loop mode or dynamically modulated by the PID controller in closed-loop mode, while shielding gas was continuously supplied to minimize oxidation during processing.

3.3 Experimental Matrix

Three sets of experiments were designed to evaluate thermal stability, melt-pool behavior, and build morphology under both open-loop and closed-loop operation. First, single-line tracks were scanned without powder feed based on set parameters shown in Table 3. During closed-loop operation, the laser power continuously adjusted to maintain each temperature setpoint; the resulting average powers (647.1, 804.8, 995.5, and 1204.8 W) were then applied as fixed powers as shown in Table 4 for the corresponding open-loop tests (Fig. 4A).

Second, single-line tracks were deposited with powder using a feed rate of 11.9 g/min and 3 L/min carrier gas based on process parameters summarized in Table 5. In this case, closed-loop control again modulated power dynamically, and the average values obtained (455.9, 777.5, 1196.8, and 1499.9 W) were used as fixed inputs for the open-loop trials as summarized in Table 6. The resulting melt-pool behavior under closed-loop and open-loop conditions is illustrated in Fig. 4B.

Finally, thin-wall structures were fabricated using a 15-layer single-bead strategy at 900 mm/min, 11.9 g/min powder feed, and 3 L/min carrier gas as shown in Fig. 4C. The closed-loop trial maintained a 1800 °C temperature setpoint with dynamically varying power, while the open-loop trial applied a fixed power of 1200 W. Collectively, these experiments provide a comprehensive comparison of thermal behavior, geometric stability, and resulting material properties under open-loop and closed-loop control.

3.4 Post-Process Characterization

Post-process characterization was performed to quantitatively assess the geometric fidelity, microstructural features, and hardness response of deposits produced under open-loop and closed-loop thermal control. Geometric evaluation was first conducted using a Micro-Epsilon scanCONTROL 3000-25 2D laser scanner, which enabled non-contact measurement of bead profiles and layer-height evolution. The scanner provided high-resolution cross-sectional maps of single-bead deposits, allowing precise determination of

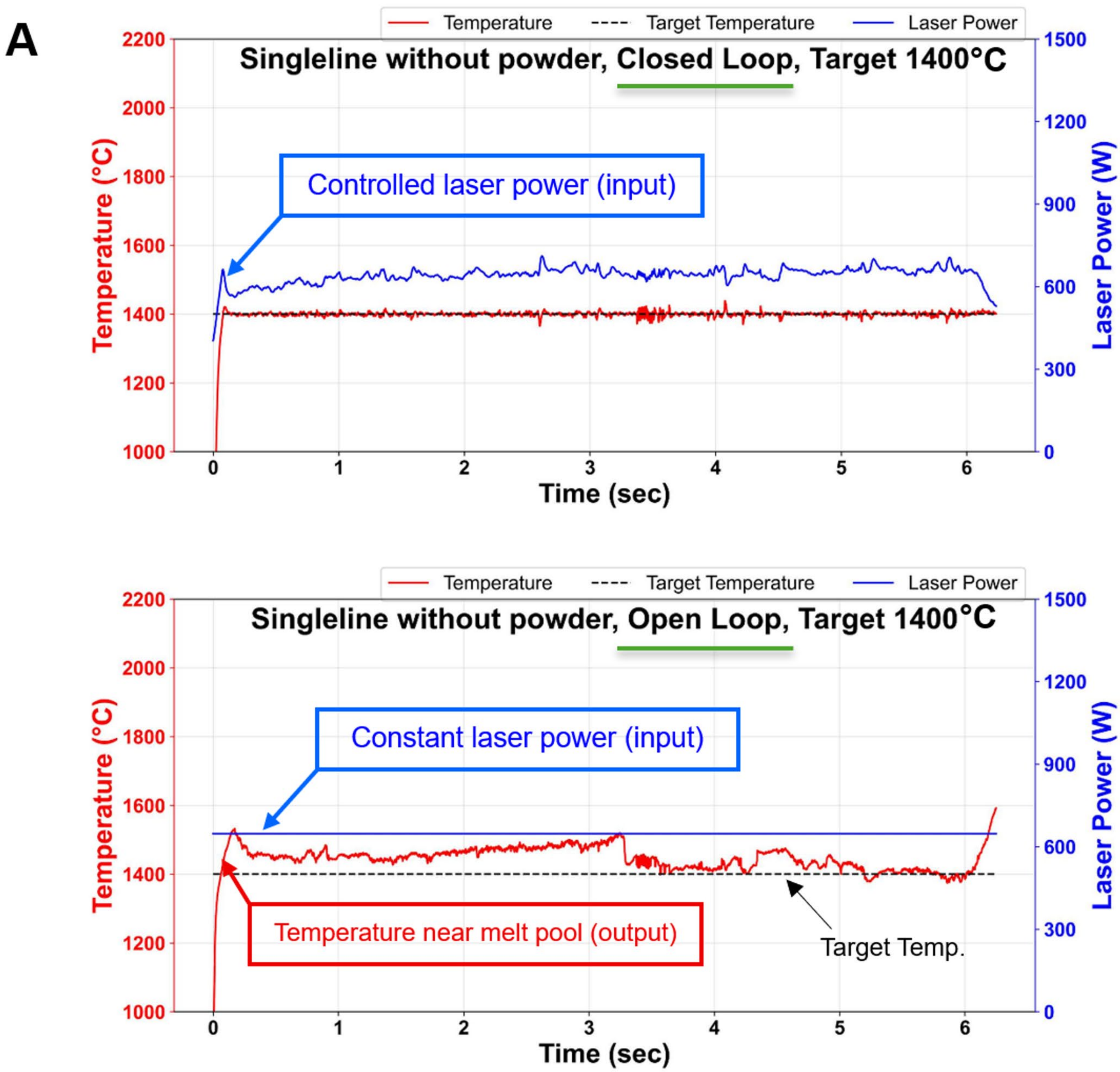

Fig. 6 Comparison of Closed-Loop and Open-Loop Temperature Control During Single-Line Laser Scans Without Powder Across Target Temperatures from (A) 1400 °C, (B) 1600 °C, and (C) 1800 °C and (D) 2000 °C

bead height, width, penetration depth, and overall morphological uniformity.

To complement the scanner-based measurements, selected single-bead and thin-wall samples were sectioned perpendicular to the scan direction and subsequently mounted, polished and etched for metallographic examination. Optical microscopy was used to see bead cross-sectional morphology, including fusion behavior, dilution characteristics, and layer-to-layer transitions. For thin-wall specimens, microstructural observations were systematically conducted at the bottom, middle, and top regions to capture vertical variations in grain morphology associated with different thermal-control modes.

Mechanical characterization was performed through Vickers microhardness mapping along the build height using a 200 g load and a 15 s dwell time. Indents were positioned to traverse the base metal, dilution zone, and deposited material to establish hardness gradients and quantify

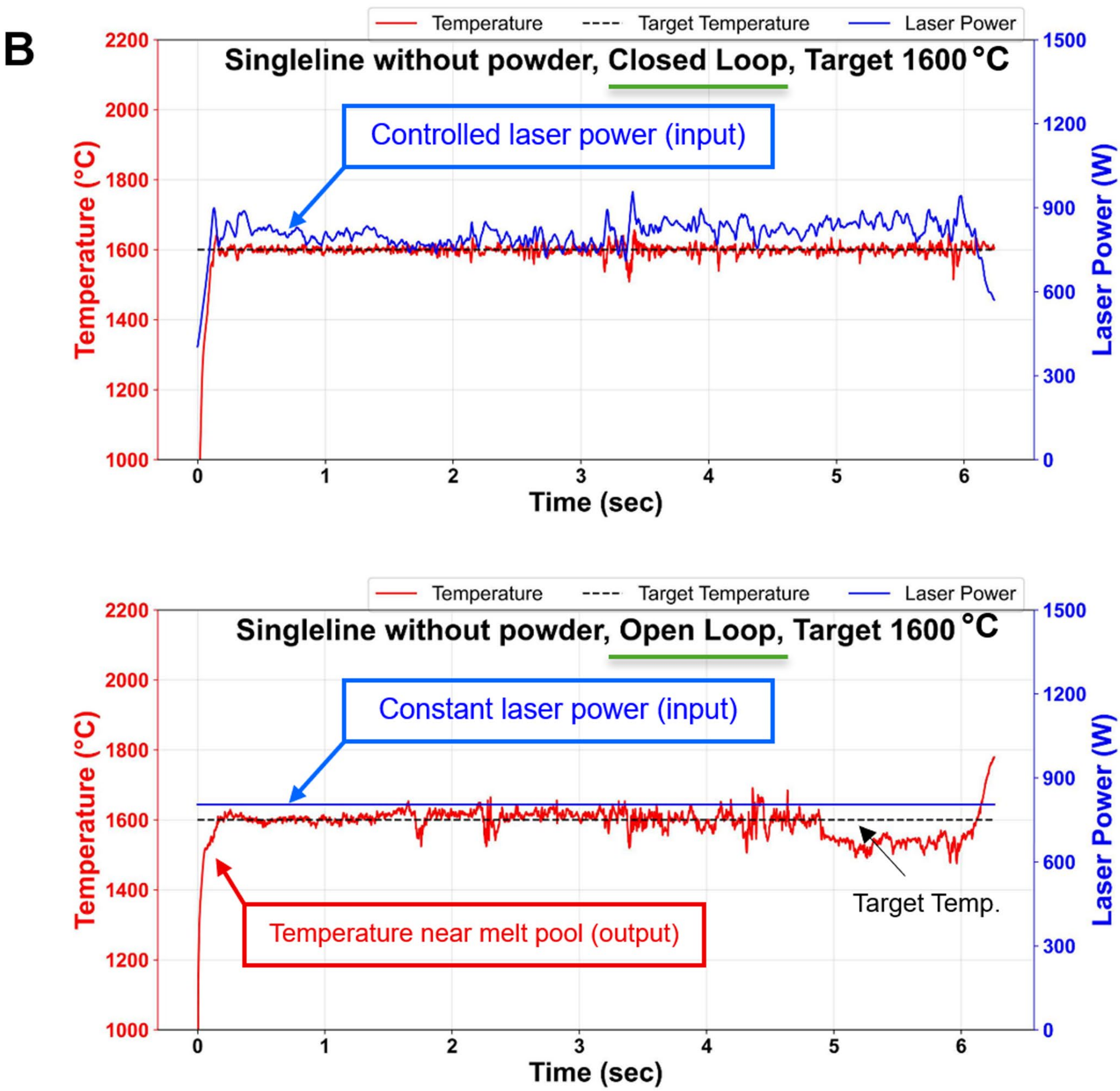

Fig. 6 (continued)

through-thickness mechanical response. The specific spatial arrangement of these measurement points, referred to as the indentation loci, is illustrated in Fig. 5, showing the systematic mapping from the substrate through the 15 deposited layers. The combination of geometric scanning, metallographic examination, and hardness profiling provided an integrated methodological framework for evaluating the influence of thermal-control strategy on solidification structure and mechanical performance.

4 Results and Discussion

4.1 Single-Line Laser melting

The temperature responses obtained at the four target setpoints are presented in Fig. 6A-D. These results reveal clear differences in the thermal behavior of the process under closed-loop and open-loop operation. At 1400 °C, shown in Fig. 6A, the closed-loop system converged to the target

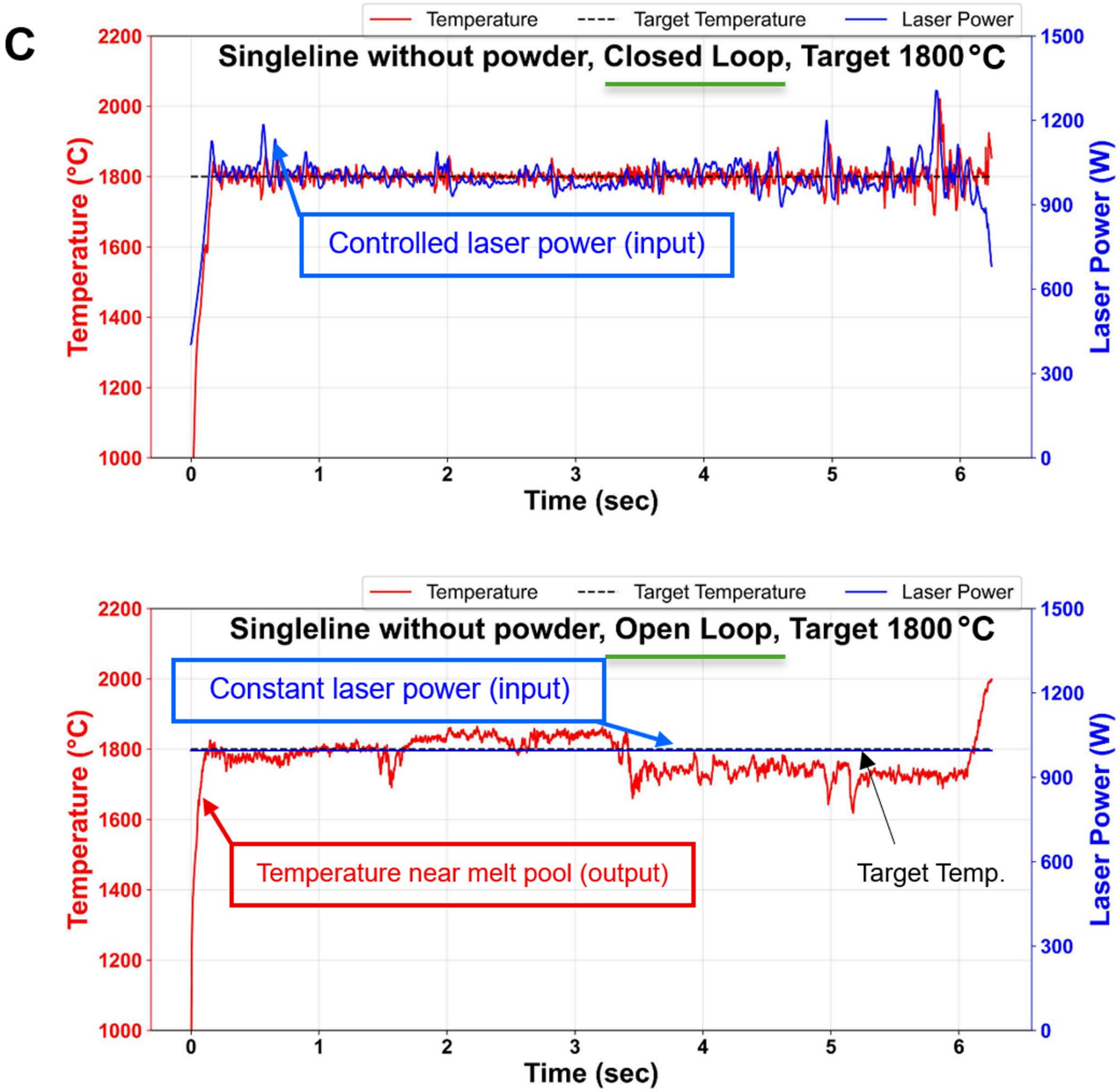

Fig. 6 (continued)

quickly and then maintained a nearly uniform temperature along the scan length. Once the initial transient had settled, the measured temperature closely matched the setpoint, demonstrating stable regulation of the melt pool. The open-loop condition, in contrast, settled at approximately 1445 °C. Although the temperature remained steady, the persistent offset indicates that constant power cannot compensate for natural variations in heat absorption and conduction during the scan.

The behavior observed at the intermediate temperatures reinforces this trend. As shown in Fig. 6B and C, the closed-loop controller continued to regulate the melt-pool temperature effectively as the thermal demand increased. The temperature profiles at 1600 °C and 1800 °C remained close to their respective targets, even though the laser power varied continually as the controller responded to small disturbances. This continuous adjustment was necessary to counteract localized changes in surface conditions and

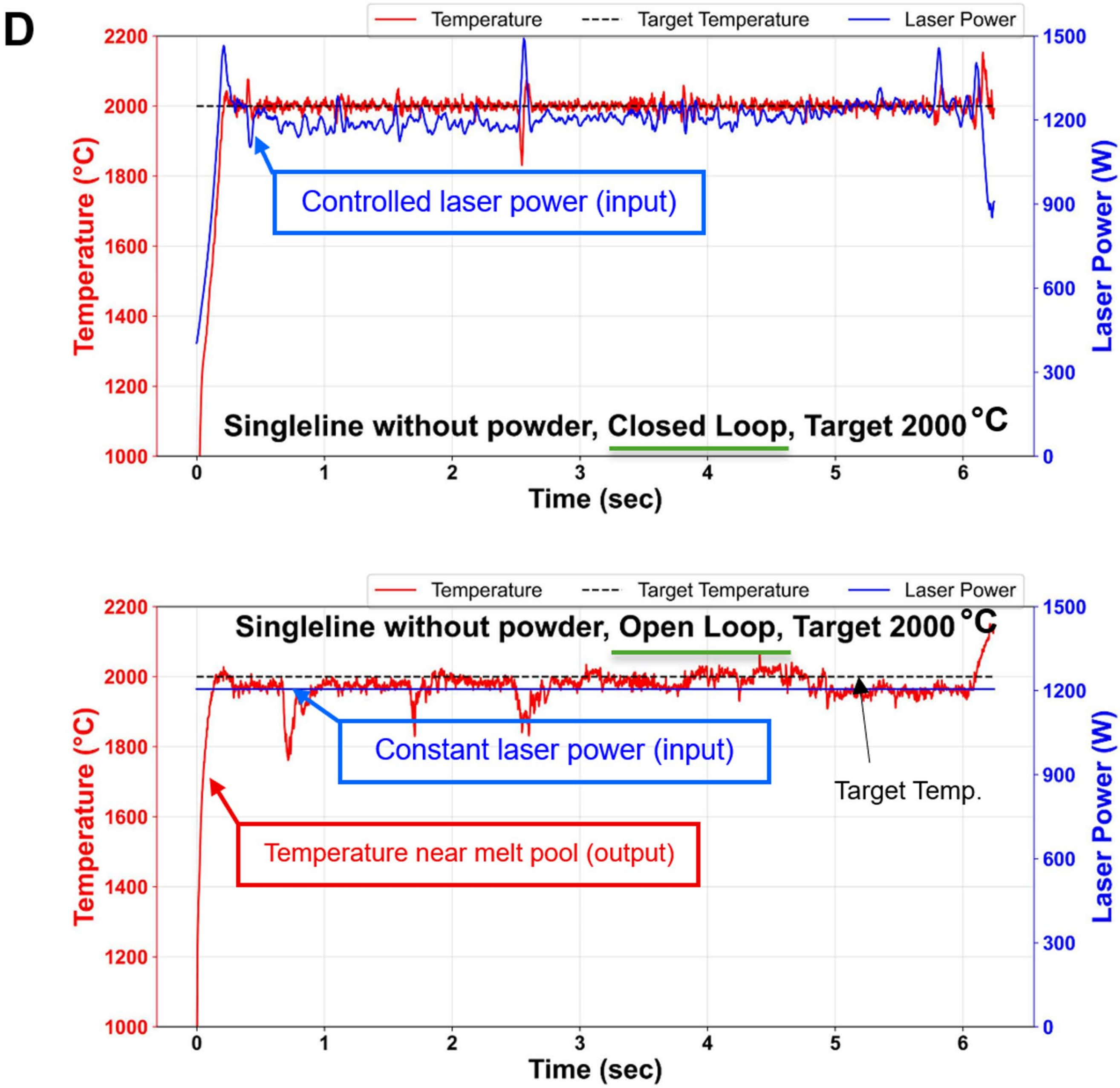

Fig. 6 (continued)

thermal gradients along the scan path. The open-loop scans at the same temperatures, however, did not maintain this level of stability. At 1600 °C the temperature drifted gradually over the length of the scan, and at 1800 °C the melt pool stabilized with a noticeably larger deviation from the intended setpoint. These results underscore that fixed power does not provide the corrective ability required to maintain thermal equilibrium as the melt pool becomes more sensitive to fluctuating conditions.

The differences between the two control approaches become even more apparent at the highest temperature. In Fig. 6D, the closed-loop system succeeded in holding the melt-pool temperature near 2000 °C despite the much larger and more rapid power adjustments required at this level. The temperature profile remained close to the target throughout the scan, indicating that the controller was able to balance rapid heat accumulation with equally rapid dissipation into the substrate. The open-loop condition,

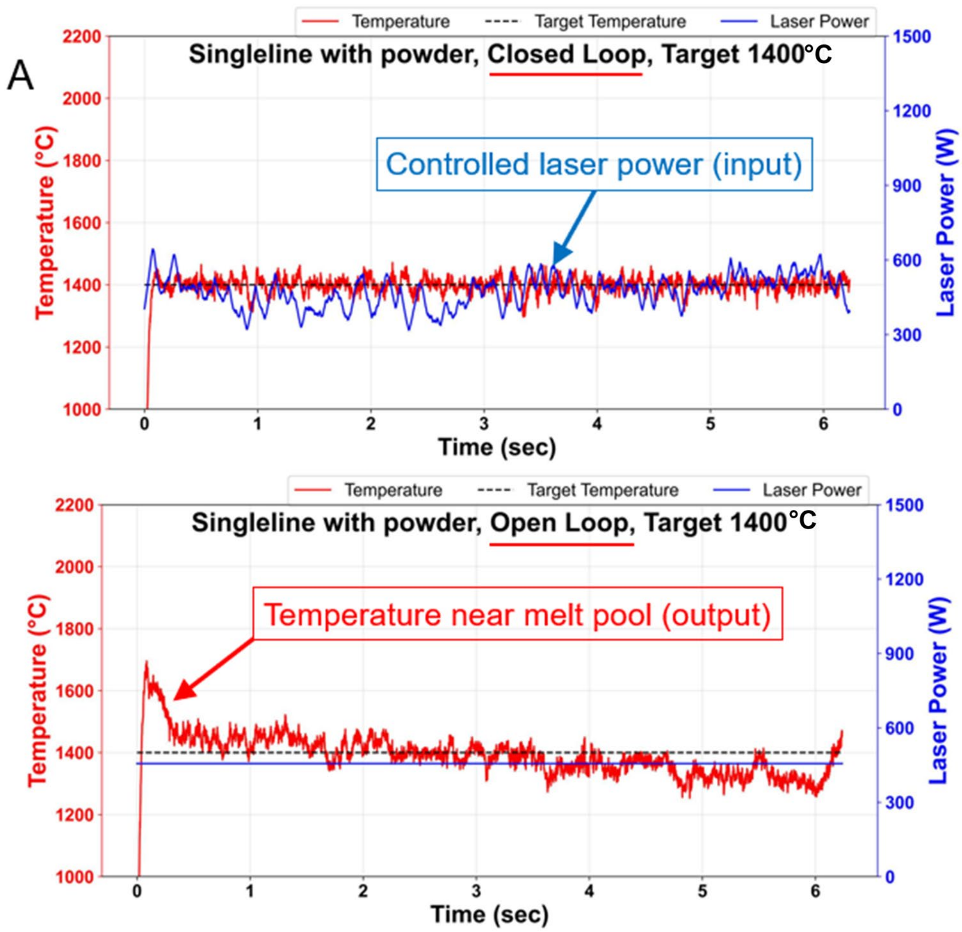

Fig. 7 Thermal response of single-line deposition with powder under closed-loop and open-loop control at target temperatures of 1400 °C (A), 1600 °C (B), 1800 °C (C), and 2000 °C (D)

meanwhile, produced a distinct hump-shaped profile rather than a stable plateau. This shape reflects progressive heating followed by a slow decline, revealing that constant power cannot accommodate the evolving thermal gradients present at higher energy densities.

4.2 Single-Line Deposition

The introduction of powder feeding noticeably changed the thermal behavior of the process, as the particles absorbed and attenuated the laser energy before reaching the substrate. Despite this added complexity, the closed-loop controller maintained stable temperature regulation across all setpoints, while the open-loop response again showed clear signs of thermal imbalance as shown in Fig. 7A and D. At the lowest target temperature (Fig. 7A), the open-loop condition exhibited a pronounced overshoot, rising to nearly 1700 °C before settling, whereas the closed-loop controller reached 1400 °C quickly and held it with minimal fluctuation. This overshoot reflects the reduced initial thermal inertia and the additional melting energy required by the powder, both of which a fixed-power setting cannot accommodate. As the temperature increased to 1600 °C and 1800 °C (Fig. 7B **and C**), the closed-loop system continued to track the targets reliably through continuous power adjustment, while the open-loop melt pool drifted around the setpoint, demonstrating limited ability to stabilize when powder absorption became more dominant. At 2000 °C (Fig. 7D), the gap widened further: the closed-loop system preserved the intended temperature despite operating near the laser's upper power limits, while the open-loop condition displayed slower convergence and growing instability.

The geometric consequences of these thermal differences are reflected clearly in the bead morphology measured by the 2D scanner (Table 7). Closed-loop deposition produced a predictable increase in bead width with temperature, rising from 1.813 mm at 1400 °C to 2.927 mm at 2000 °C. This monotonic trend aligns with the expected behavior of

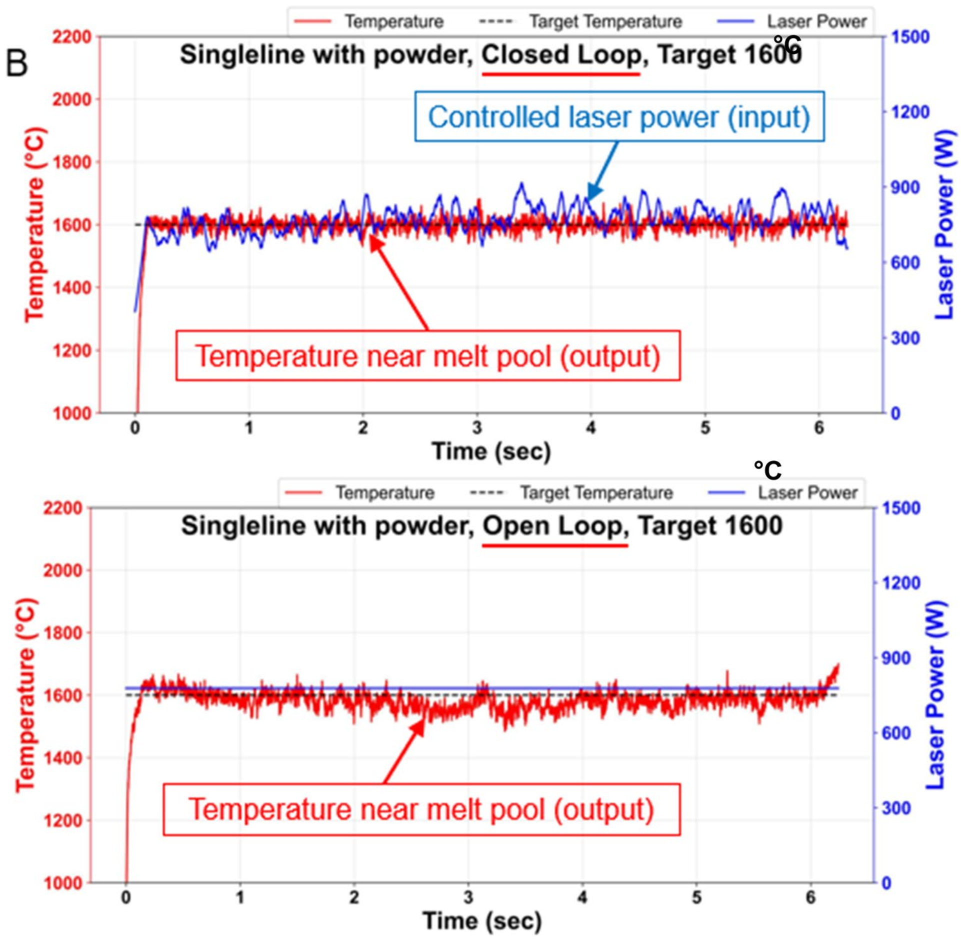

Fig. 7 (continued)

a hotter, lower-viscosity melt pool that spreads more readily across the substrate. The open-loop samples did not follow this predictable pattern. At 1400 °C, the open-loop width remained narrow at 1.575 mm, consistent with the insufficient wetting caused by the initial thermal overshoot and the subsequent inability to maintain the required energy input. At higher temperatures, the open-loop beads widened but did so inconsistently, and their width–height ratios varied more than in the closed-loop condition. These fluctuations indicate that the geometric profile was directly influenced by the unstable thermal response observed in Fig. 7B and D. Figure 8 shows the resulting bead cross-sections.

4.3 Thin-Wall Deposition

The 15-layered thin-wall experiment provided a clear view of how cumulative heat affects melt-pool behavior during vertical build-up. Under open-loop operation with a fixed laser power of 1196.8 W, the melt-pool temperature rose continuously from 1726 °C in the first layer to 2028 °C by the fifteenth layer, producing more than 300 °C of uncontrolled thermal drift. This gradual temperature escalation led to increasingly unstable melt-pool shapes and inconsistent bead height. The progression is evident in Fig. 9, where the temperature curve steepens with each successive layer, reflecting the accumulation of heat that the fixed-power system could not counteract.

Figure 10A shows that the closed-loop control strategy, operating at a target melt-pool temperature of 1800 °C, exhibits a highly stable thermal response compared with the open-loop condition. In the open-loop case, the process operates at a nearly constant laser power of approximately 1200 W while the melt-pool temperature increases progressively with build height, indicating cumulative heat

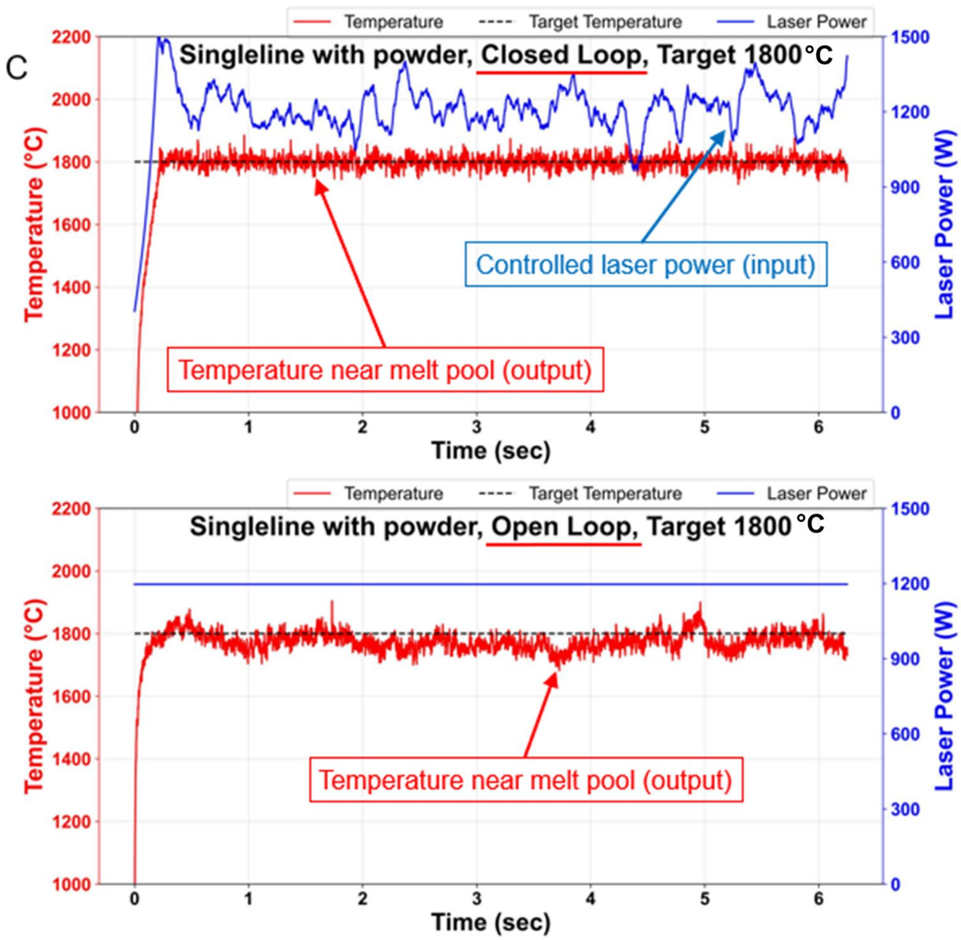

Fig. 7 (continued)

accumulation in the absence of active thermal regulation. Under closed-loop control, the system rapidly compensates for heat buildup during the layers by reducing the laser power from approximately 1500 W to below 800 W. As deposition progresses and heat accumulation increases with wall height, the controller dynamically compensates for layer-to-layer thermal fluctuations by modulating the laser power within a low range of approximately 400–650 W, with several layers operating below 700 W. Despite these substantial reductions in energy input, the melt-pool temperature remains consistently regulated near the target value throughout the entire 15-layer build, demonstrating the effectiveness of closed-loop thermal feedback in maintaining process stability while minimizing energy input.

In this study, the term 'cell size' refers specifically to the sub-grain cellular structures and Secondary Dendrite Arm Spacing (SDAS). These features are established metallurgical indicators for the local cooling rate in 316 L stainless steel DED processes. This distinction is critical, as these sub-grain features—rather than primary grain boundaries—directly reflect the high-frequency thermal stabilization achieved by the closed-loop controller.

The hardness profiles plotted in Fig. 10B demonstrate that the open-loop wall exhibited wide variability, ranging from 180 to 240 HV, with the lowest values occurring in regions where the microstructure had coarsened due to accumulated heat and reduced cooling rates. The downward trend in the open-loop hardness curve toward the top of the wall mirrors the thermal runaway observed during deposition, confirming that uncontrolled melt-pool morphology leads to diminished microhardness. In contrast, the closed-loop wall maintained consistently higher hardness between 210 and 240 HV and displayed a stable upward trend across the build height, reflecting the finer, more uniform dendritic structure preserved by active temperature regulation. This observation is further corroborated by Fig. 10C, which shows that

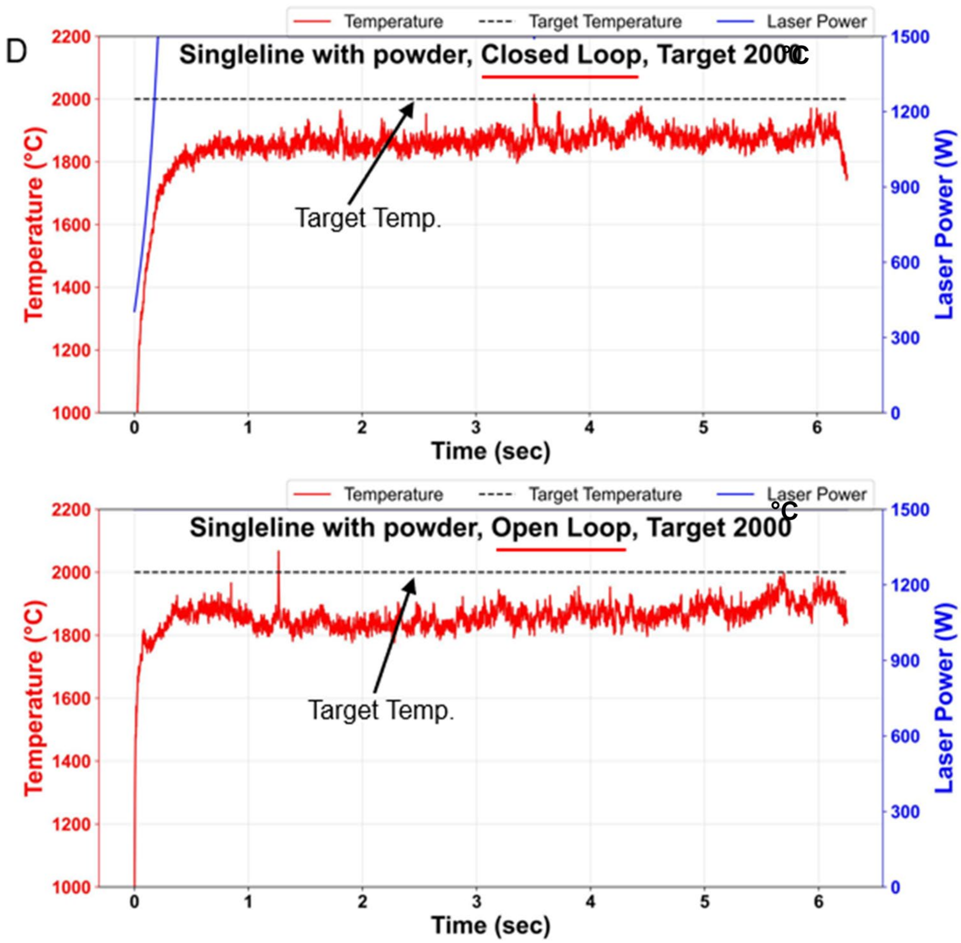

Fig. 7 (continued)

Table 7 Geometric Comparison (Closed Loop vs. Open Loop)

Test No.	Target Temp (°C)	CL Width (mm)	CL Height (mm)	OL Width (mm)	OL Height (mm)
1	1400	1.813	0.537	1.575	0.676
2	1600	1.866	0.585	2.168	0.683
3	1800	2.477	0.801	2.333	0.796
4	2000	2.927	0.769	2.698	0.682

the closed-loop process maintains a consistently smaller and more uniform cell size along the build height, whereas the open-loop condition exhibits increasing scatter and coarsening toward the top of the wall. This refinement, together with the suppression of excessive epitaxial grain growth, produced a more homogeneous microstructure. Overall, the roughly 20–30% increase in hardness relative to the open-loop condition highlights the significant mechanical advantage gained by preventing thermal drift and maintaining a stable thermal environment during thin-wall fabrication.

While the controller maintained the target temperature successfully, a minor upward trend in laser power was observed during the final three layers (Layers 13–15). This behavior is attributed to the inherent limitations of the off-axis pyrometer configuration. As the build height increases, even with Z-axis compensation to maintain a fixed 19 mm standoff distance, slight variations in the viewing angle or optical alignment relative to the melt pool center can occur. These minor misalignments cause the sensor to register a perceived temperature slightly lower than the actual peak. Consequently, the incremental PID controller—tuned to prioritize error elimination —automatically increased the laser power to compensate for this perceived drop. This observation highlights a known constraint of off-axis sensing in tall geometries and suggests that future work involving significantly taller builds may benefit from coaxial monitoring to ensure angle-independent thermal readings.

The microstructural contrast between the two thin walls directly reflects the different thermal histories imposed by

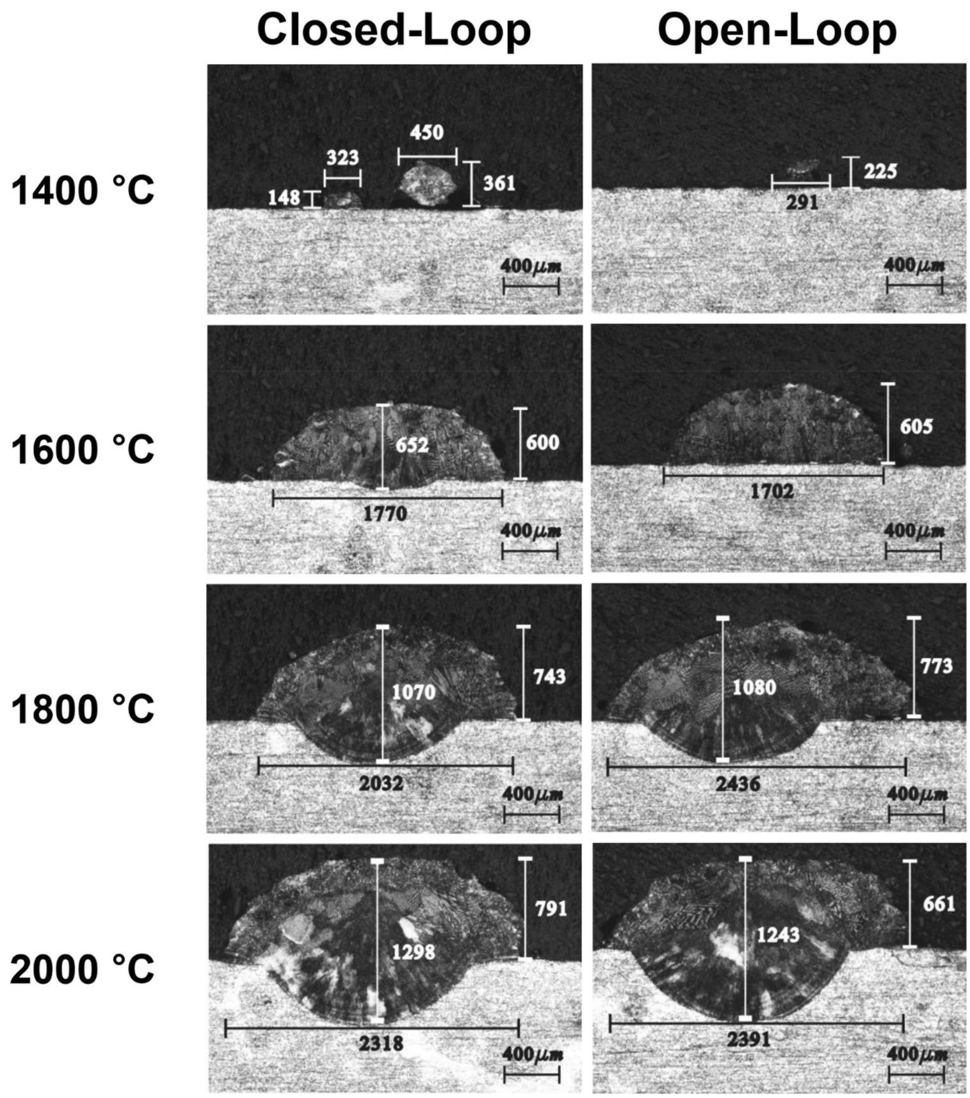

Fig. 8 Geometric Comparison of Cross-Sections of deposited specimens during temperature ranges (1400–2000 °C) for Closed Loop and Open Loop

open-loop and closed-loop operation. In the open-loop wall, the cumulative temperature rise of more than 300 °C produced markedly coarse, elongated grains throughout the build height. The top region shows large, irregular grains exceeding 5 µm in secondary arm spacing, while the mid- and lower regions retain similarly coarse and strongly epitaxial structures, indicating sustained overheating and a collapse of the thermal gradient. In contrast, the closed-loop wall exhibits a consistently refined cellular dendrite morphology, with arm spacings decreasing from approximately 3.0 µm near the top to about 2.68 µm in the lower layers. This uniform refinement is a direct consequence of stabilizing the melt-pool temperature by limiting heat accumulation and maintaining higher effective cooling rates, the closed-loop system suppressed grain coarsening and prevented the upward propagation of columnar structures. As shown in Fig. 11, the closed-loop process therefore yields a much more homogeneous and mechanically favorable microstructure than the open-loop counterpart.

A distinctive narrowing of the deposit width with increasing height is observed in the closed-loop specimen (Fig. 11), a trend that contrasts with the open-loop wall. This geometric evolution is a direct consequence of the active thermal regulation strategy. In open-loop mode, the constant 1200 W laser power leads to progressive heat accumulation, which maintains or widens the melt pool as vertical heat dissipation becomes restricted. Conversely, the closed-loop controller effectively suppresses thermal runaway by drastically modulating the laser power—reducing it from an initial 1500 W to approximately 450–650 W in the final layers—to maintain the stable 1800°C setpoint. This significant reduction in energy density results in a narrower and more

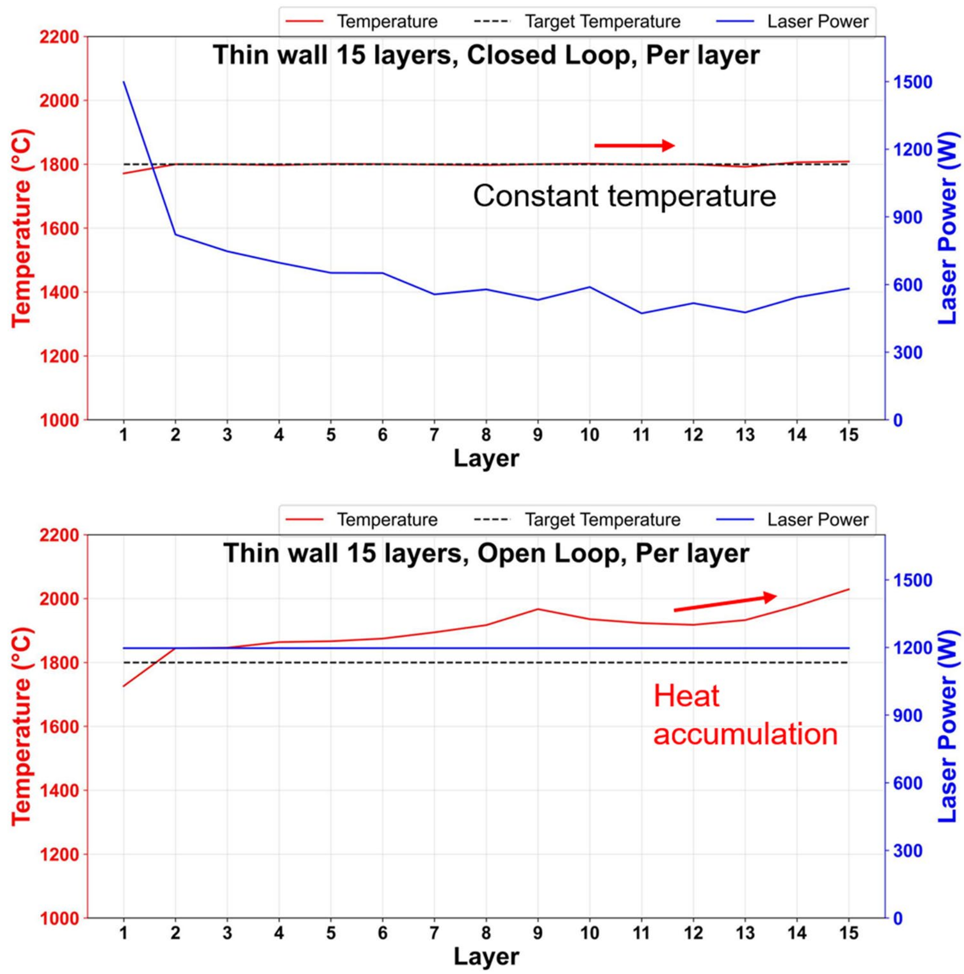

Fig. 9 Thermal response during Thin wall deposition during Closed Loop (Top) and Open Loop(bottom)

controlled melt pool, ensuring geometric consistency and preventing the 'mushrooming' effect typically associated with cumulative heat buildup in DED.

Across all experiments from single-line scans to thin-wall builds, the developed ALOHA-DED system consistently demonstrated stable melt-pool regulation, predictable geometry, refined microstructure, and improved mechanical performance when operated in closed-loop mode. The controller maintained accurate and fast temperature tracking across a wide thermal window, prevented heat accumulation during long and multi-layer deposits. These behaviors directly translated into uniform bead geometry, finer dendritic structures, and hardness levels 20–30% higher than open-loop deposition. The present results therefore validate that the ALOHA-DED system, despite its low hardware complexity and affordability, achieves process stability and material performance comparable to those of significantly more expensive commercial systems.

5 Conclusions

This study demonstrated that real-time melt-pool temperature regulation is the key determinant of thermal stability, geometric consistency, microstructural refinement, and mechanical performance in DED. Across single-line and thin-wall builds, the closed-loop controller maintained accurate temperature tracking over a wide process window, prevented more than 300 °C of thermal drift during multi-layer deposition. These stabilized thermal conditions produced predictable bead geometry, refined dendritic microstructures, and hardness values 20–30% higher than those achieved under open-loop operation. The strong correlation between thermal control and material outcomes observed here agrees closely with prior findings on commercial DED systems, yet was achieved on a low-cost, open-architecture ALOHA-DED platform. This confirms that high-fidelity thermal control does not require expensive proprietary hardware, and that open systems can deliver research-grade process stability. The validated platform provides a robust

Fig. 10 **(A)** Evolution of average melt-pool temperature and laser power, **(B)** microhardness distribution **(C)** Cell size (representing sub-grain cellular structure/SDAS) versus Height across deposited layers under closed-loop and open-loop control

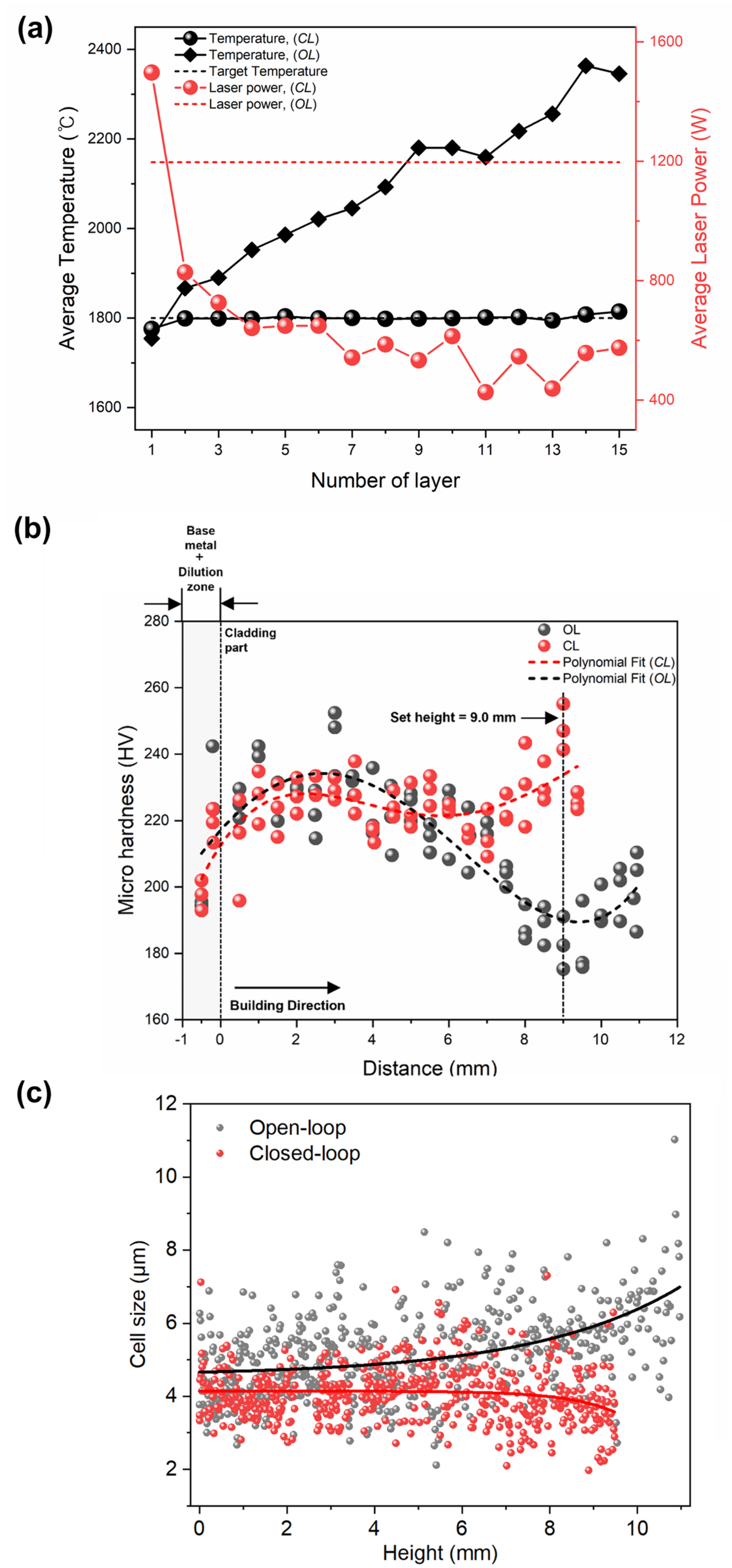

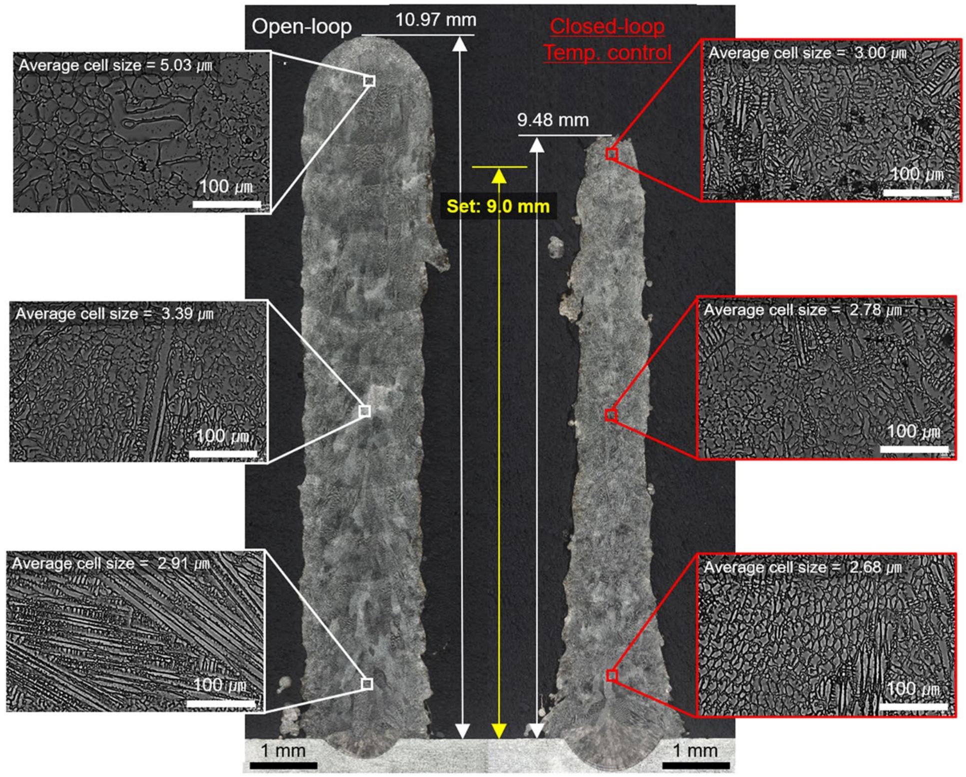

Fig. 11 Comparison of microstructure. Left (OL) shows coarser sub-grain cellular growth due to heat accumulation. Right (CL) shows refined sub-grain structure due to active power regulation

foundation for future work in adaptive DED control, including multi-variable regulation of speed, mass flow, and bead height, as well as real-time defect mitigation and autonomous process optimization.

Supplementary Information The online version contains supplementary material available at https://doi.org/10.1007/s40684-026-00909-2.

Acknowledgements This research was supported by Korea Basic Science Institute (National research Facilities and Equipment Center) grant funded by the Ministry of Education. (grant No. 2021R1A6C101A449) and supported by the National Research Foundation of Korea(NRF) grant funded by the Korea government(MSIT) (No. RS-2023-NR076859).

Declaration

Conflict of interest The authors declare that they have no known competing financial interests or personal relationships that could have appeared to influence the work reported in this paper.

References

1. Thompson, S. M., Bian, L., Shamsaei, N., & Yadollahi, A. (2015). An overview of Direct Laser Deposition for additive manufacturing; Part I: Transport phenomena, modeling and diagnostics. *Additive Manufacturing*, *8*, 36–62. https://doi.org/10.1016/J.ADDMA.2015.07.001
2. Li, C., Liu, Z. Y., Fang, X. Y., & Guo, Y. B. (2018). Residual Stress in Metal Additive Manufacturing. *Procedia CIRP*, *71*, 348–353. https://doi.org/10.1016/J.PROCIR.2018.05.039
3. Svetlizky, D., Das, M., Zheng, B., Vyatskikh, A. L., Bose, S., Bandyopadhyay, A., Schoenung, J. M., Lavernia, E. J., & Eliaz, N. (2021). Directed energy deposition (DED) additive manufacturing: Physical characteristics, defects, challenges and applications. *Materials Today*, *49*, 271–295. https://doi.org/10.1016/J.MATTOD.2021.03.020
4. Ye, L., Xue, H., Li, Z., Zhou, Y., Chen, G., Xu, F., Melentiev, R., Newman, S., & Yu, N. (2025). Review of online quality control for laser directed energy deposition (LDED) additive manufacturing. *International Journal of Extreme Manufacturing*. https://doi.org/10.1088/2631-7990/aded4f. 7.
5. Imran, M. M., Che Idris, A., De Silva, L. C., Kim, Y. B., & Abas, P. E. (2024). Advancements in 3D Printing: Directed Energy Deposition Techniques, Defect Analysis, and Quality Monitoring. *Technologies*, *12*. https://doi.org/10.3390/technologies12060086
6. Li, S. H., Kumar, P., Chandra, S., & Ramamurty, U. (2023). Directed energy deposition of metals: processing, microstructures, and mechanical properties. *International Materials Reviews*, *68*, 605–647. https://doi.org/10.1080/09506608.2022.2097411/FORMAT/EPUB
7. Muvvala, G., Patra Karmakar, D., & Nath, A. K. (2017). Online monitoring of thermo-cycles and its correlation with microstructure in laser cladding of nickel based super alloy. *Optics and Lasers in Engineering*, *88*, 139–152. https://doi.org/10.1016/J.OPTLASENG.2016.08.005
8. Nair, A. M., Muvvala, G., Sarkar, S., & Nath, A. K. (2020). Real-time detection of cooling rate using pyrometers in tandem in laser material processing and directed energy deposition. *Materials Letters*, 277. https://doi.org/10.1016/j.matlet.2020.128330
9. Song, L., & Mazumder, J. (2011). Feedback control of melt pool temperature during laser cladding process. *IEEE Transactions on Control Systems Technology*, *19*, 1349–1356. https://doi.org/10.1109/TCST.2010.2093901

10. Bernauer, C. J., Zapata, A., Kick, L., Weiss, T., Sigl, M. E., & Zaeh, M. F. (2022). Pyrometry-based closed-loop control of the melt pool temperature in Laser Metal Deposition with coaxial wire feeding. *Procedia CIRP*, *111*, 296–301. https://doi.org/10.1016/j.procir.2022.08.025
11. Smoqi, Z., Bevans, B. D., Gaikwad, A., Craig, J., Abul-Haj, A., Roeder, B., Macy, B., Shield, J. E., & Rao, P. (2022). Closed-loop control of meltpool temperature in directed energy deposition. *Materials and Design*, 215. https://doi.org/10.1016/j.matdes.2022.110508
12. Liao, S., Jeong, J., Zha, R., Xue, T., & Cao, J. (2023). Simulation-guided feedforward-feedback control of melt pool temperature in directed energy deposition. *CIRP Annals*, *72*, 157–160. https://doi.org/10.1016/j.cirp.2023.03.014
13. Chen, Z., Guo, X., & Shi, J. (2021). Hardness Prediction and Verification Based on Key Temperature Features During the Directed Energy Deposition Process. *International Journal of Precision Engineering and Manufacturing - Green Technology*, *8*, 453–469. https://doi.org/10.1007/s40684-020-00208-4
14. Sanchez-Medina, J., De Baere, D., Snyers, C., Jardon, Z., Hinderdael, M., Ertveldt, J., & Guillaume, P. (2023). Comparison and analysis of hyperspectral temperature data in directed energy deposition. *Journal of Laser Applications*, *35*, 42037. https://doi.org/10.2351/7.0001074/2916228
15. Lee, K. K., Kim, J., Moon, S. K., & Ahn, D. G. (2025). Prediction of the Bead Shape in a Directed Energy Deposition Process Using Machine Learning with Limited Point Data. *International Journal of Precision Engineering and Manufacturing - Green Technology*. https://doi.org/10.1007/s40684-025-00795-0
16. Tang, L., & Landers, R. G. (2011). Layer-to-layer height control for laser metal deposition process. *Journal of Manufacturing Science and Engineering*. https://doi.org/10.1115/1.4003691. 133.
17. Sanchez-Medina, J., Jardon, Z., Snyers, C., Hinderdael, M., Guillaume, P., & De Baere, D. (2024). FPGA real-Time melt-pool temperature control in Directed Energy Deposition. *Procedia CIRP*, *124*, 318–323. https://doi.org/10.1016/j.procir.2024.08.126
18. Sanchez-Medina, J., De Baere, D., Snyers, C., Jardon, Z., Hinderdael, M., Ertveldt, J., & Guillaume, P. (2023). Comparison and analysis of hyperspectral temperature data in directed energy deposition. *Journal of Laser Applications*, *35*. https://doi.org/10.2351/7.0001074
19. Hansen, K. P., & Broeng, J. (2006). High-power photonic crystal fiber lasers. *Photonics Spectra*.
20. Miyato, T., Kayahara, T., Fujisaki, A., Furukawa, K., Matsushita, M., Muramatsu, M., Harada, Y., & Niino, H. (2014). High power single-mode fiber laser and its application to metal and non-metal materials. *Proceedings of SPIE - The International Society for Optical Engineering*, *8963*, 89630W. https://doi.org/10.1117/12.2036570
21. Parker, F., Martino-Gauchi, F., O'Brien, C., Conneely, A., & O'Connor, G. M. (2008). A study of high-speed remote micro-processing with a galvanometer based fiber laser. *ICALEO 2008–27th International Congress on Applications of Lasers and Electro-Optics, Congress Proceedings*.
22. Kancharla, V. (2004). Fiber lasers for industrial cutting applications. *ICALEO 2004–23rd International Congress on Applications of Laser and Electro-Optics Congress Proceedings*. https://doi.org/10.2351/1.5060266
23. Naeem, M., & Lewis, S. (2006). Micro joining and cutting with a single mode fiber laser. *PICALO 2006–2nd Pacific International Conference on Applications of Laser and Optics - Conference Proceedings*, *400–405*. https://doi.org/10.2351/1.5056971
24. Wang, W., & Li, L. (2011). High-quality high-material-usage multiple-layer laser deposition of nickel alloys using sonic or ultrasonic vibration powder feeding. *Proceedings of the Institution of Mechanical Engineers Part B: Journal of Engineering Manufacture*, *225*, 130–139. https://doi.org/10.1177/09544054JEM2128
25. Wang, W., Pinkerton, A. J., & Li, L. (2008). A gas-free powder delivery system for 100% deposition efficiency in Direct Laser Deposition. *ICALEO 2008–27th International Congress on Applications of Lasers and Electro-Optics Congress Proceedings*, 415–423. https://doi.org/10.2351/1.5061341
26. Yuan, Y., Yu, K., Zhu, H., & Ehmann, K. F. (2022). Continuous feeding of powders with vibration and pneumatic pressure assistance for laser-based additive manufacturing processes. *Journal of Manufacturing Processes*, *82*, 336–346. https://doi.org/10.1016/j.jmapro.2022.08.002
27. Zou, J., Xie, S., Zhu, B., Liu, T., Fang, C., & Zhuang, Y. (2025). Effect of material surface states in the laser spot on the absorptivity during laser melting processing. *Applied Surface Science*, 688. https://doi.org/10.1016/j.apsusc.2025.162384
28. Zhao, L., Wang, L., Li, G., Zhu, G., & Shi, S. (2020). Research Progress on Coaxial Powder Feeding Nozzle for Laser Metal Additive Manufacturing. *Laser and Optoelectronics Progress*, *57*. https://doi.org/10.3788/LOP57.050002
29. Wang, Z., Zhang, A., & Shang, X. (2009). 3-D Design and Numerical Simulation of Two-Phase Flow in the Laser Rapid Prototyping Coaxial Powder Delivery System. *Tsinghua Science and Technology*, *14*, 200–205. https://doi.org/10.1016/S1007-0214(09)70092-6
30. Yezi, L., Cheng, X., & Sun, J. (2013). Fuzzy PID controller combines with closed-loop optimal fuzzy reasoning for pitch control system. *Proceedings of SPIE - The International Society for Optical Engineering*, *8783*, 87830W. https://doi.org/10.1117/12.2013926
31. Onuseit, V., Boley, S., Brinkmeier, D., Peter, A., Menold, T., Hagenlocher, C., Graf, T., & Michalowski, A. (2024). Enhancing stability in thin-walled part production with L-DED wire using an adaptive controller. *Procedia CIRP*, *124*, 305–308. https://doi.org/10.1016/j.procir.2024.08.123
32. Torres-Garcia, D., Mendez-Barrios, C. F., & Niculescu, S. I. (2024). Impact of Delay-Difference Approximation on PID Controllers: Stability and Performance Insights. *2024 32nd Mediterranean Conference on Control and Automation, MED 2024*, 616–621. https://doi.org/10.1109/MED61351.2024.10566201
33. Chen, J., Lv, Z., Zhang, X., Xu, T., & Cheng, Y. (2025). Temperature Control of Quartz-Glass Melting Areas in Laser Additive Manufacturing. *Micromachines*, *16*. https://doi.org/10.3390/mi16010029
34. Bernauer, C. J., Zapata, A., Kick, L., Weiss, T., Sigl, M. E., & Zaeh, M. F. (2022). Pyrometry-based closed-loop control of the melt pool temperature in Laser Metal Deposition with coaxial wire feeding. *Procedia CIRP*, *111*, 296–301. https://doi.org/10.1016/j.procir.2022.08.025
35. Zhang, W., Yang, M., Li, G., & Soshi, M. (2025). Productive Energy Fluence (PEF) controller using feed and laser hybrid control for Directed Energy Deposition (DED). *Journal of Manufacturing Processes*, *142*, 1–17. https://doi.org/10.1016/j.jmapro.2025.03.047
36. Ali, N., Tomesani, L., Ascari, A., & Fortunato, A. (2022). Fabrication of Thin Walls with and without Close Loop Control as a Function of Scan Strategy Via Direct Energy Deposition. *Lasers in Manufacturing and Materials Processing*, *9*, 81–101. https://doi.org/10.1007/s40516-022-00164-8